PRL 119, 058002 (2017) PHYSICAL REVIEW LETTERS week ending 4 AUGUST 2017

Collective Behavior of Chiral Active Matter: Pattern Formation and Enhanced Flocking

Benno Liebchen[1,*] and Demian Levis[2,3,†]
[1]SUPA, School of Physics and Astronomy, University of Edinburgh, Edinburgh EH9 3FD, United Kingdom
[2]Departament de Física de la Matèria Condensada, Universitat de Barcelona, Martí i Franquès 1, E08028 Barcelona, Spain
[3]Universitat de Barcelona Institute of Complex Systems (UBICS), Universitat de Barcelona, E08028 Barcelona, Spain

(Received 20 January 2017; revised manuscript received 11 May 2017; published 1 August 2017)

We generalize the Vicsek model to describe the collective behavior of polar circle swimmers with local alignment interactions. While the phase transition leading to collective motion in 2D (flocking) occurs at the same interaction to noise ratio as for linear swimmers, as we show, circular motion enhances the polarization in the ordered phase (enhanced flocking) and induces secondary instabilities leading to structure formation. Slow rotations promote macroscopic droplets with late time sizes proportional to the system size (indicating phase separation) whereas fast rotations generate patterns consisting of phase synchronized microflocks with a controllable characteristic size proportional to the average single-particle swimming radius. Our results defy the viewpoint that monofrequent rotations form a vapid extension of the Vicsek model and establish a generic route to pattern formation in chiral active matter with possible applications for understanding and designing rotating microflocks.

DOI: 10.1103/PhysRevLett.119.058002

Among the most remarkable features of active matter systems is their ability to spontaneously form self-sustained nonequilibrium structures, without requiring external driving. These structures range from motility-induced phase separation of self-propelled particles into a dense and a dilute phase [1,2] and clusters of self-limited size [3–7] in isotropic active matter to long range ordered flocks and traveling bands in 2D polar active matter [8–12]. Despite their phenomenological diversity, most of these (and other) activity-induced structures can be observed in a small class of archetypical minimal models allowing us to explore their universality. For linear self-propelled particles which change their swimming direction only by diffusion (and alignment interactions), the active Brownian particle model and the Vicsek model have become standard models representing isotropic and polar active matter.

Besides such linear swimmers, there is now a strong interest in a new class of self-propelled particles which change their direction of motion autonomously. This class of chiral active matter includes a variety of biological circle swimmers, such as *E. coli*, which swim circularly when close to walls and interfaces [13–16], as well as sperm cells [17,18], and magnetotactic bacteria in rotating external fields [19,20]. Following the general principle that any deviation between the self-propulsion direction of the particle and its symmetry axis couples its translational and rotational degrees of freedom, it has also been possible to design synthetic circle swimmers; examples being L-shaped self-phoretic swimmers [21,22] and actuated colloids allowing us to design radius and frequency of circular trajectories on demand. While these synthetic examples have supported the recent boost of interest in chiral active matter, as the recent reviews [23,24] reflect, surprisingly little is known about their collective behavior (exceptions exploring collective behavior are [25–27]).

Therefore, following the spirit of formulating minimal models for the collective behavior of linear active matter, here, we introduce the *chiral active particle* model (CAP) to describe the collective behavior of polar circle swimmers. The CAP model describes overdamped self-propelled particles changing their direction autonomously with an intrinsic rotation frequency, and due to local alignment interactions between circle swimmers (which are typically nonspherical). In the monochromatic case of identical circle swimmers, one might expect that circular swimming has little impact on the physics of the Vicsek model, as the absence of inertia seems to guarantee invariance of the system by global rotation of the reference frame—as for an overdamped ideal gas in a rotating bucket, where global rotations do not change the particle dynamics inside. This viewpoint receives further support from the fact that the flocking transition of Vicsek models proves invariant under rotations, as we will show. Strikingly, however, as a distinct active matter effect, this flocking transition induces long-range polar order in 2D, which spontaneously breaks rotational invariance. The consequence is that uniform rotations, as a seemingly minor modification of the Vicsek model, become nontrivial in this symmetry-broken state and induce a new phase consisting of rotating microflocks. These microflocks emerge at a characteristic length scale which can be qualitatively predicted at a mean-field level and controlled via the swim speed and the rotational frequency of the underlying circle swimmers. This allows us to use rotations as a tool to design microflock patterns.

Besides fast rotations, slow ones also induce new collective effects: they allow for large-scale aggregates of phase-locked circle swimmers which scale linearly with system size and feature an enhanced polarization as compared to uniform flocks in the Vicsek model. Following their sizes and shapes, we call them macrodroplets. Thus, contrasting the obvious viewpoint that monofrequent rotations do not change the collective behavior of linear swimmers significantly, the present work shows that they generate a rich new route to pattern formation. This route should be readily observable in identical synthetic circle swimmers (L-shaped or actuated colloids) or in magnetotactic bacteria in rotating external magnetic fields, and could be useful, for example, to design localized microflocks whose characteristic size can be (dynamically) controlled in the laboratory (e.g., by changing the self-propulsion velocity or the frequency of the applied field).

Besides this, our results may find further applications for understanding pattern formation in 2D suspensions of sperm cells [18] and driven protein filaments [26,28] qualitatively matching the microflocks we observe. Note that our results may qualitatively apply even to nonidentical but synchronized biological swimmer ensembles [27].

The chiral active particle model.—To specify our results, we now define the CAP as a rotating and smooth variant of the Vicsek model in continuous time [10,29,30]: it consists of N pointlike self-propelled particles with positions $\mathbf{r}_i$ and orientations $\mathbf{p}_i(t) = (\cos\theta_i, \sin\theta_i)$ which interact via an aligning pair potential and change their direction in response to a systematic rotational force, according to

$$\dot{\mathbf{r}}_i = v\mathbf{p}_i,$$
$$\dot{\theta}_i = \omega + \frac{K}{\pi R_\theta^2}\sum_{j\in\partial_i}\sin(\theta_j - \theta_i) + \sqrt{2D_r}\eta_i, \qquad (1)$$

Here, the sum runs over neighbors within a radius R_θ around particle i, and $\eta_i(t)$ is a unit-variance Gaussian white noise with zero mean. In the noninteracting limit ($K = 0$), each particle performs an overdamped circular Brownian motion as shown in Fig. 1 and statistically characterized in [31]. To reduce the parameter space to its essential dimensions, we choose space and time units as R_θ and $1/D_r$. The CAP model has four control parameters: the particle density $\rho_0 = NR_\theta^2/L^2$, a Péclet number $\mathrm{Pe}_r = v/(D_r R_\theta)$ measuring the persistence length in units of the alignment interaction range, $g = K/(\pi R_\theta^2 D_r)$, and $\Omega = \omega/D_r$, comparing alignment and rotational frequencies with the rotational diffusion rate. Remarkably, the phase diagram is determined predominantly by only two of these parameters, $g\rho_0$ and Ω, as we discuss below. Interesting phenomena occur for $g_f \coloneqq g\rho_0 > 2$ and for $\Omega \sim 1$ or $\Omega > 1$. Hence, a sufficiently large number of circle swimmers ($N \sim 10^3$–10^4), sedimented on a quadratic surface of linear size $L \sim 10^2$–10^3 μm above the standard flocking transition of the Vicsek model [32] should allow us to explore our phase diagram: Rotating *E.coli* ($\omega \sim 0.1$–$1/\mathrm{s}$ [15]; $D_r \sim 0.2/\mathrm{s} - 1/\mathrm{s}$) lead to $\Omega \sim 1$, whereas L-shaped swimmers ($\omega \sim 0.1 - 0.3/\mathrm{s}$; $D_r \sim 6.10^{-4}$ [21]) allow us to explore the regime $\Omega \sim 10^2 \gg 1$, and magnetotactic bacteria in rotating fields should allow us to tune Ω on demand.

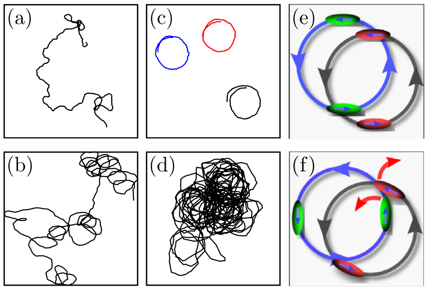

FIG. 1. Trajectory of an isolated linear [(a), $\Omega = 0$] and circle swimmer [(b), $\Omega = 3$]. Trajectories of circle swimmers in the macrodroplet [(c), $g\rho_0 = 2.8$, $\Omega = 0.2$] and the microflock phase [(d), $g\rho_0 = 2.8$, $\Omega = 3$]. (e) and (f) are cartoons illustrating the mechanism underlying macrodroplet and microflock formation: for slow rotations, circle swimmers phase-lock and follow circular orbits allowing for aligned configurations and the formation of large rotating clusters (e), whereas fast rotations frustrate the alignment interactions (f).

Pattern formation.—We now simulate the collective behavior of N identical circle swimmers in a quadratic box with periodic boundary conditions (see [33] for details). For $\Omega = 0$, we reproduce the phenomenology of the Vicsek model [12,35–37]: a disordered homogeneous phase occurs below the flocking threshold ($g < g_f$), whereas $g \gtrsim g_f$ induces a global polarization with high density bands coexisting with a disordered gas [Fig. 2(a)]. Stronger couplings eventually destabilize these bands and induce homogeneous flocking. Now, choosing $g > g_f$ and switching on slow rotations ($\Omega = 0.2$), we observe a separation of circle swimmers into a polarly ordered and almost spherical dense phase (macrodroplet) and an incoherent low-density gas, resembling the usual liquid-gas demixing. This droplet rotates coherently but slower than individual swimmers with a frequency $\Omega^* < \Omega$ [see Figs. 1(c), 2(b), and Movie 1 in the Supplemental Material (SM) [33]] and grows, at late times, linearly with the system size [33], indicating phase separation. Tuning the frequency to values $\Omega \gtrsim 1$ leads, strikingly, to a pattern of dense clusters emerging with a characteristic (and system-size independent) length scale [see Figs. 2(c)–2(h) and Movie 3 [33]]. Within each cluster, particles synchronize and form rotating microflocks: hence, we call the emerging phase the rotating microflock pattern. This pattern resembles vortex arrays observed in sperm cells and protein filaments [18,28].

Hydrodynamic equations and enhanced flocking.—To understand the emergence of patterns and their length

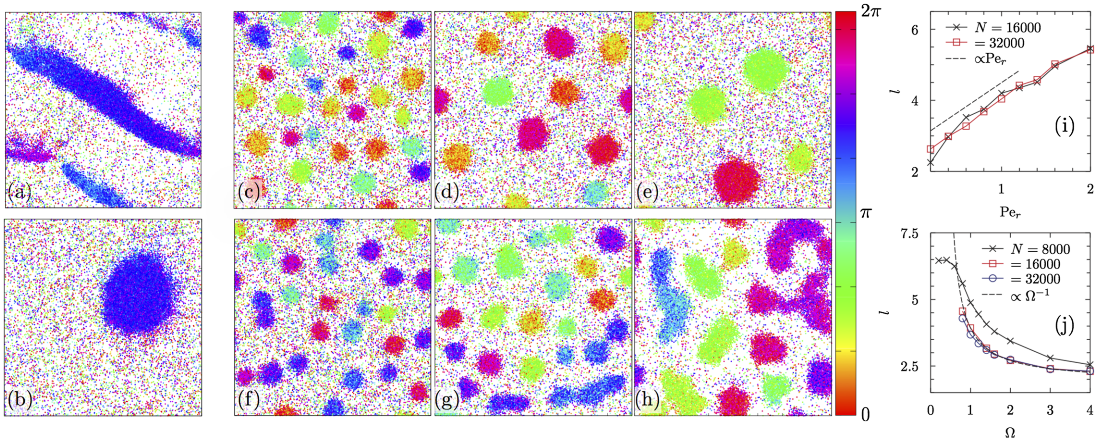

FIG. 2. Simulation snapshots for $N = 32\,000$ particles with colors encoding particle orientations. [(a), $\Omega = 0$]: Traveling bands; [(b), $\Omega = 0.2 < 1$]: rotating macrodroplet (phase separation) (c)–(h): Microflock pattern at $g\rho_0 = 2.8$, $\Omega = 3$, and $\mathrm{Pe}_r = 0.2$ (c), $\mathrm{Pe}_r = 1.0$ (d), and $\mathrm{Pe}_r = 2$ (e), and at $\mathrm{Pe}_r = 0.2$, $\Omega = 3$, and $g\rho_0 = 2.4$ (f), 3.6 (g), and 6 (h). (i), (j): Microflock length scale l for $g\rho_0 = 2.8$; for $\Omega = 3$ as a function of Pe_r (i), and for $\mathrm{Pe}_r = 0.2$ as a function of Ω (j) for the system sizes shown in the key.

scales, we derive a continuum theory for the CAP model in the SM [33]. Following the approaches in [38,39], we find a closed set of equations for the particle density $\rho(\mathbf{x}, t)$ and polarization density $\mathbf{w}(\mathbf{x}, t) = (w_x, w_y) = \rho\mathbf{P}$ [with $\mathbf{P}(\mathbf{x}, t)$ being the polarization field] where $|\mathbf{w}|$ measures the local degree of alignment and $\mathbf{w}/|\mathbf{w}|$ the average swimming direction

$$\dot{\rho} = -\mathrm{Pe}_\mathrm{r}\boldsymbol{\nabla}\cdot\mathbf{w}, \tag{2}$$

$$\begin{aligned}\dot{\mathbf{w}} = {} & (g\rho - 2)\frac{\mathbf{w}}{2} - \frac{\mathrm{Pe}_\mathrm{r}}{2}\boldsymbol{\nabla}\rho + \frac{\mathrm{Pe}_\mathrm{r}^2}{2b}\nabla^2\mathbf{w} - \frac{g^2}{b}|\mathbf{w}|^2\mathbf{w} \\ & + \frac{g\mathrm{Pe}_\mathrm{r}}{4b}[5\boldsymbol{\nabla}\mathbf{w}^2 - 10\mathbf{w}(\boldsymbol{\nabla}\cdot\mathbf{w}) - 6(\mathbf{w}\cdot\nabla)\mathbf{w}] \\ & + \Omega\mathbf{w}_\perp + \frac{\mathrm{Pe}_\mathrm{r}^2\Omega}{4b}\boldsymbol{\nabla}^2\mathbf{w}_\perp - \frac{g^2\Omega}{2b}|\mathbf{w}|^2\mathbf{w}_\perp \\ & - \frac{g\mathrm{Pe}_\mathrm{r}\Omega}{8b}[3\boldsymbol{\nabla}_\perp\mathbf{w}^2 - 6\mathbf{w}(\boldsymbol{\nabla}_\perp\cdot\mathbf{w}) - 10(\mathbf{w}\cdot\boldsymbol{\nabla}_\perp)\mathbf{w}]. \end{aligned} \tag{3}$$

Here, $b = 2(4 + \Omega^2)$, $\mathbf{w}_\perp = (-w_y, w_x)$, and $\boldsymbol{\nabla}_\perp = (-\partial_y, \partial_x)$. First, we note that the disordered uniform phase D $(\rho, \mathbf{w}) = (\rho_0, \mathbf{0})$ solves (3) with ρ_0 being the particle density. Linearizing (3) around phase D (SM [33]), unveils an instability (flocking transition) $g\rho_0 > 2$, which is the same as for linear swimmers ($\Omega = 0$) showing that the emergence of long-range order is invariant to rotations. Our simulations confirm this invariance (Fig. 3) [40]. Following the flocking instability, the CAP approaches a rotating uniform phase called the F phase, $(\rho, |\mathbf{w}|, \mathbf{w}/|\mathbf{w}|) = (\rho_0, w_0, \cos(\Omega_0 t), \sin(\Omega_0 t))$, featuring long-range order

$$w_0 = \frac{1}{g}\sqrt{(g\rho_0 - 2)(4 + \Omega^2)}. \tag{4}$$

In this phase, a macroscopic fraction of circle swimmers phase-synchronizes and rotates coherently with a frequency $\Omega_0 = \Omega[\frac{3}{2} - (g\rho_0/4)]$. This frequency reduces to the single particle frequency at the onset of flocking, but slows down as $g\rho_0$ increases. Remarkably, (4) suggests that the polarization increases with Ω, a phenomenon which we call enhanced flocking and confirm numerically in Fig. 3 for locally uniform macrodroplets (in [33] we also confirm enhanced flocking for phase F alongside the predicted slowdown of rotations). Physically, enhanced flocking might be based on a decrease of the average time needed for a diffusive rotating particle (which is not yet part of the flock) to align its direction with the flock. That is, rotations allow the flock to collect particles with random orientations faster.

Microflock instability.—Phase F is stable only at very large $g\rho_0$ ([33]) but features secondary instabilities creating the patterns described above. To understand their emergence, we now perform a linear stability analysis of phase F. Here, the presence of long-range order in the base state allows terms of order $\Omega\mathbf{w}\boldsymbol{\nabla}_\perp\mathbf{w}$ to crucially impact its stability. First, considering the case $\Omega = 0$, we find an oscillatory long wavelength instability along the polarization direction for $2 < g\rho_0 < 22/7$ (and a stationary long wavelength instability perpendicular to the flocking direction for $2 < g\rho_0 < 82/21$). The oscillatory instability

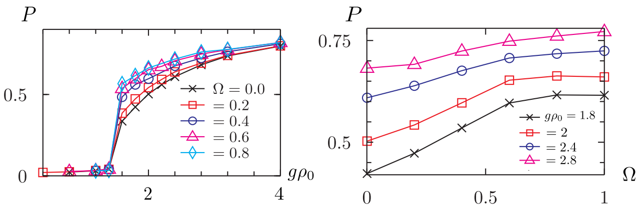

FIG. 3. Global polarization over $g\rho_0$ and Ω showing invariance of the flocking transition against rotations (left) and enhanced flocking (right) as predicted in the text.

evokes moving density fluctuations only in the polarization direction and is often associated with the emergence of traveling bands in the Vicsek model [37,39]. In the CAP, we also find oscillatory long wavelength instabilities, here, producing moving density fluctuations both longitudinal and perpendicular to the flocking direction which might be responsible for the emergence of (coarsening) macrodroplets [Fig. 2(b)].

Most strikingly, for larger Ω, our linear stability analysis ([33]) unveils a rotation-induced oscillatory short wavelength instability which generates pattern formation in the CAP and explains the observation of microflocks with a characteristic size [Fig. (2)]; hence, we call it the microflock instability. Close to $g\rho_0 = 2$, the size of emerging microflocks scales as (see [33])

$$l \approx \frac{\pi \mathrm{Pe}_r}{2\Omega^2} \frac{|4(2 - g\rho_0) + \Omega^2(12 - g\rho_0)|}{\sqrt{(g\rho_0 - 2)(4 + \Omega^2)}}. \tag{5}$$

Thus, microflocks grow linearly with Pe_r and typically decrease with Ω. If $\Omega \gg 1$, (5) yields $l \propto v/\omega$, predicting microflock sizes proportional to the (average) radius of a single circle swimmer. Our simulations confirm these scalings [Figs. 2(i) and 2(j)]: Specifically, defining the length scale l of a numerically observed structure as the value where the pair correlation function $G(l) = 1$ leads to Fig. 2: panel 2(i) confirms the $l \propto \mathrm{Pe}_r$ prediction and 2(j) shows a decrease of l with increasing Ω, revealing that the microflock size can be tuned by the microscopic parameters in our model [41]. In line with (5), we also find that l only depends on $g\rho_0$, whereas the macrodroplet size depends on g and ρ_0 individually [33]. Also, in contrast to macrodroplets which saturate relatively quickly to sizes comparable to N, microflocks grow slowly and do not phase-separate macroscopically (at least) on experimentally relevant timescales [33].

What is the physical mechanism leading to the rotating droplet phase and the microflock pattern? While circle swimmers are effectively independent of each other at large distances in phase D, for $g\rho_0 > 2$ they have to satisfy the rotations while being aligned on average. If interactions dominate ($g\rho_0/\Omega \gg 1$), circle swimmers can phase lock before they rotate much and follow almost ideal circles [Fig. 1(c)]. Here, they are parallel to each other all along their circular orbits [Fig. 1(e)] and form a macroscopic rotating droplet [Fig. 2(b)]. In this state, interactions support circular motion: phase locking leads to an essentially stiffly rotating many-particle object that experiences an "average" noise, inducing only weak deviations from circular motion [Fig. 1(c)]. Conversely, when rotations dominate ($g\rho_0/\Omega < 1$), the phase locking timescale becomes comparable to the rotational timescale. This results in phase shifts among adjacent circle swimmers that frustrate, for swimmers on circular orbits, the alignment interaction [Fig. 1(f)]. The frustration, in turn, destroys circular orbits and makes large droplets of phase-locked swimmers impossible. As a result, the droplet phase breaks down opening a route to pattern formation: the resulting microflock phase can be seen as an attempt of the CAP to satisfy alignment interactions in the presence of rotations but in absence of phase-locking, at least on average [see Fig. 1(d) for a typical trajectory]: rotating around a common center allows particles to avoid close-to-orthogonal configurations such as the one shown in Fig. 1(f) even in the presence of small phase shifts.

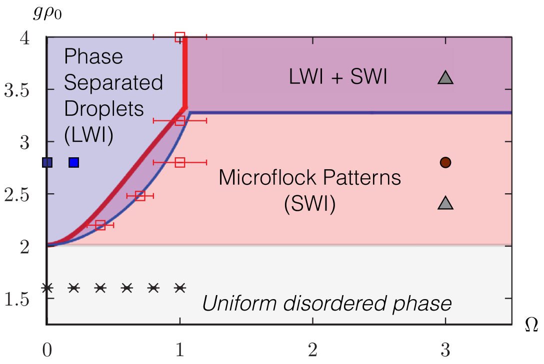

FIG. 4. Nonequilibrium phase diagram. The solid red line (obtained by linear stability analysis) and red symbols (simulations; bars represent numerical uncertainty) separate the macrodroplet phase (left, blue domain) induced by a long wavelength instability (LWI) from the microflock phase (pink domain) following an oscillatory, short wavelength instability (SWI) [33]. Overlaying colors (LWI + SWI) indicate phase coexistence. The light gray domain (bottom) represents stability of the disordered uniform phase. Black symbols show the location of the flocking transition from simulations. Filled symbols show parameters of Fig. 2: (a), (b) blue squares; (c)–(e) brown dot, (f)–(g) gray triangles.

Finally, we summarize our results from linear stability analysis and simulations in an instability or phase diagram, Fig. 4. Although the CAP model depends on four dimensionless parameters, we show in the SM [33] that the linear stability of the uniform phase is fully characterized by $g\rho_0$ and Ω. In Fig. 4, the red shaded areas lead to microflock patterns while the blue ones represent the rotating macrodroplet phase. Where both regimes overlap ($\Omega \sim 1$ and $g\rho_0 \gtrsim 10/3$), short and long wavelength instabilities perpendicular to the flocking direction coexist. Generally, we also find a coexisting long wavelength instability in the polarization direction, which is not shown in Fig. 4 but is detailed in the SM [33]. Often, the coexisting long and short wavelength instabilities are separated by a band of stable wave numbers (Fig. 1 in [33]), suggesting that, depending on initial conditions, phase F proceeds either towards a microflock pattern or towards a macrodroplet. This suggests hysteresis in the CAP: we confirm this in Movie 5 [33], showing phase separation for small Ω persisting even after a quench to large Ω values, which normally lead to the microflock pattern, when our system is initialized in phase F.

Conclusions.—Chiral active matter can feature long-range polar order in 2D (as polar active matter) which violates rotational invariance even for monofrequent rotations and induces new patterns: Slow rotations lead to coarsening macrodroplets featuring an enhanced polarization compared to the Vicsek model, whereas faster rotations induce microflock patterns with a characteristic size which can be tuned via the swimming speed and the rotation frequency of the underlying circle swimmers. This allows us to use rotations as a design principle for microflock patterns.

While microflocks and macrodroplets show various distinguishing features, including the instability in the underlying mean-field equations leading to their emergence (short- vs long-wavelength instability), the Ω- and ρ_0-dependence of their sizes [Fig. 2(j); [33]], the shape of the contained trajectories (Fig. 1), and the temporal growth-law of the largest structure ([33]), the present work does not definitely commit regarding whether or not the microflock pattern slowly phase-separates macroscopically but invites further studies to fully characterize the nature of the transition between macrodroplets and microflocks.

B. L. and D. L. gratefully acknowledge funding from a Marie Curie Intra European Fellowship (G. A. No. 654908 and G. A. No. 657517) within Horizon 2020.

B. L. and D. L. contributed equally to this work.

---

[*] Benno.Liebchen@ed.ac.uk, bliebche@gmail.com
[†] levis@ub.edu

[1] J. Tailleur and M. E. Cates, Phys. Rev. Lett. **100**, 218103 (2008).
[2] M. E. Cates and J. Tailleur, Annu. Rev. Condens. Matter Phys. **6**, 219 (2015).
[3] I. Theurkauff, C. Cottin-Bizonne, J. Palacci, C. Ybert, and L. Bocquet, Phys. Rev. Lett. **108**, 268303 (2012).
[4] J. Palacci, S. Sacanna, A. P. Steinberg, D. J. Pine, and P. M. Chaikin, Science **339**, 936 (2013).
[5] I. Buttinoni, J. Bialké, F. Kümmel, H. Löwen, C. Bechinger, and T. Speck, Phys. Rev. Lett. **110**, 238301 (2013).
[6] D. Levis and L. Berthier, Phys. Rev. E **89**, 062301 (2014).
[7] B. Liebchen, D. Marenduzzo, I. Pagonabarraga, and M. E. Cates, Phys. Rev. Lett. **115**, 258301 (2015).
[8] T. Vicsek, A. Czirók, E. Ben-Jacob, I. Cohen, and O. Shochet, Phys. Rev. Lett. **75**, 1226 (1995).
[9] J. Toner and Y. Tu, Phys. Rev. Lett. **75**, 4326 (1995).
[10] F. D. C. Farrell, M. C. Marchetti, D. Marenduzzo, and J. Tailleur, Phys. Rev. Lett. **108**, 248101 (2012).
[11] J.-B. Caussin, A. Solon, A. Peshkov, H. Chaté, T. Dauxois, J. Tailleur, V. Vitelli, and D. Bartolo, Phys. Rev. Lett. **112**, 148102 (2014).
[12] A. P. Solon, H. Chaté, and J. Tailleur, Phys. Rev. Lett. **114**, 068101 (2015).
[13] H. C. Berg and L. Turner, Biophys. J. **58**, 919 (1990).
[14] W. R. DiLuzio, L. Turner, M. Mayer, P. Garstecki, D. B. Weibel, H. C. Berg, and G. M. Whitesides, Nature (London) **435**, 1271 (2005).
[15] E. Lauga, W. R. DiLuzio, G. M. Whitesides, and H. A. Stone, Biophys. J. **90**, 400 (2006).
[16] R. Di Leonardo, D. DellArciprete, L. Angelani, and V. Iebba, Phys. Rev. Lett. **106**, 038101 (2011).
[17] B. M. Friedrich and F. Jülicher, Proc. Natl. Acad. Sci. U.S.A. **104**, 13256 (2007).
[18] I. H. Riedel, K. Kruse, and J. Howard, Science **309**, 300 (2005).
[19] K. Ērglis, Q. Wen, V. Ose, A. Zeltins, A. Sharipo, P. A. Janmey, and A. Cēbers, Biophys. J. **93**, 1402 (2007).
[20] A. Cēbers, J. Magn. Magn. Mater. **323**, 279 (2011).
[21] F. Kümmel, B. ten Hagen, R. Wittkowski, I. Buttinoni, R. Eichhorn, G. Volpe, H. Löwen, and C. Bechinger, Phys. Rev. Lett. **110**, 198302 (2013).
[22] B. ten Hagen, F. Kümmel, R. Wittkowski, D. Takagi, H. Löwen, and C. Bechinger, Nat. Commun. **5**, 4829 (2014).
[23] H. Löwen, Eur. Phys. J. Spec. Top. **225**, 2319 (2016).
[24] B. Friedrich, Eur. Phys. J. Spec. Top. **225**, 2353 (2016).
[25] A. Kaiser and H. Löwen, Phys. Rev. E **87**, 032712 (2013).
[26] J. Denk, L. Huber, E. Reithmann, and E. Frey, Phys. Rev. Lett. **116**, 178301 (2016).
[27] B. Liebchen, M. E. Cates, and D. Marenduzzo, Soft Matter **12**, 7259 (2016).
[28] M. Loose and T. J. Mitchison, Nat. Cell Biol. **16**, 38 (2014).
[29] F. Peruani, A. Deutsch, and M. Bär, Eur. Phys. J. Spec. Top. **157**, 111 (2008).
[30] O. Chepizhko and F. Peruani, Phys. Rev. Lett. **111**, 160604 (2013).
[31] S. van Teeffelen and H. Löwen, Phys. Rev. E **78**, 020101 (2008).
[32] Following Onsager theory, for particles with a large aspect ratio ($\gtrsim 10$), steric repulsion should be sufficient to generate (local) alignment at moderate area fractions ($\gtrsim 0.2$).
[33] See Supplemental Material http://link.aps.org/supplemental/10.1103/PhysRevLett.119.058002 for further details, which includes the additional Refs. [34,35].
[34] A. Gopinath, M. F. Hagan, M. C. Marchetti, and A. Baskaran, Phys. Rev. E **85**, 061903 (2012).
[35] T. Vicsek and A. Zafeiris, Phys. Rep. **517**, 71 (2012).
[36] G. Grégoire and H. Chaté, Phys. Rev. Lett. **92**, 025702 (2004).
[37] S. Mishra, A. Baskaran, and M. C. Marchetti, Phys. Rev. E **81**, 061916 (2010).
[38] D. S. Dean, J. Phys. A **29**, L613 (1996).
[39] E. Bertin, M. Droz, and G. Grégoire, J. Phys. A **42**, 445001 (2009).
[40] We find a flocking transition close to, but slightly below, the theoretical prediction, as previously noted in [10].
[41] In Fig. 2(j), we only show l within the regime where microflocks are approximately isotropic. For larger g, the length scale l, as defined by the pair correlation function, depends on the microflock shape and does not represent their length scale in a unique way.